Teknik Dergi, 2022 12163-12182, Paper 676

Experimental Study of Hydrodynamic Pressures Acting on a Submerged Gate

Sochheat SMOK[1]
Mehmet Anil KIZILASLAN[2]
Adnan Tolga KURUMUS[3]
Ender DEMİREL[4]

ABSTRACT

Vortical flow formed by a submerged hydraulic jump may produce significant hydrodynamic lift and drag pressures on a gate beneath the hydraulic jump. In this study, an experimental setup equipped with multi-pressure sensors was used to measure fluctuating impact pressures on the submerged gate for different flow conditions characterized by the inlet Froude number and submergence factor (S). Time-averaged and instantaneous pressure coefficients are evaluated based on simultaneous measurements of wall pressures at multiple locations, including those at the lip and downstream face of the gate. In particular, instantaneous lift pressure coefficients are observed to be independent of the submergence ratio for $S > 0.6$. It is found that low Froude number flows produce high surface pressure fluctuations and the dominant frequency of pressure fluctuations shifts to higher frequency as the Froude number increases. Pressure measurements for the free hydraulic jump suggest that the power spectra of lift pressure fluctuations are devoid of any significant energy level, whereas the resulting power spectra of the submerged flow exhibits significant energy level in the frequency range of 14-19 Hz. The proposed measurement system can be used for the in situ identification of hydrodynamic pressures acting on the gates in irrigation canals.

Keywords: Submerged gate, pressure sensor, hydrodynamic impact, pressure coefficient.

Note:
- This paper has been received on March 23, 2020 and accepted for publication by the Editorial Board on January 18, 2021.
- Discussions on this paper will be accepted by September 30, 2022.
- https://doi.org/10.18400/tekderg.707668

1 Civil Engineer (MSc), Cambodia - smok.sochheat@gmail.com – https://orcid.org/0000-0001-9662-3517

2 Çanakkale Onsekiz Mart University, Construction Department, Çanakkale, Turkey - makizilaslan@comu.edu.tr - https://orcid.org/0000-0002-0621-4646

3 Eskişehir Osmangazi University, Civil Engineering Department, Eskişehir, Turkey - tolgakurumus@gmail.com - https://orcid.org/0000-0002-2694-067X

4 Eskişehir Osmangazi University, Civil Engineering Department, Eskişehir, Turkey - edemirel@ogu.edu.tr - https://orcid.org/0000-0002-0440-7866

1. INTRODUCTION

Gates are the most common hydraulic structures not only to control the flow but also to measure the flow discharge in streams under free and submerged flow conditions. Submerged hydraulic jump occurs downstream of a vertical gate when the tail water depth exceeds conjugate subcritical depth of the free hydraulic jump.

This results in less air-water interaction and energy dissipation than that in the free jump. Interaction of the backward flow with the mean flow creates spatially and temporally varying vortices in the roller region downstream of the control structure. Prediction of vortex-induced hydrodynamic forces acting on the gate is important in design stage since the interaction of incoming jet with the recirculating flow in the roller region may cause the breakdown of the control structure depending on the flow conditions that develop.

Most of the experimental studies conducted in the literature consist of measuring instantaneous velocity components by using Acoustic Doppler Velocimetry (ADV), Particle Image Velocimetry (PIV) by Amir et al. [1] and Laser Doppler Anemometry (LDA) by Svendsen et al. [2]. Turbulent flow downstream of a submerged gate develops in a three-dimensional flow structure and strong fluctuations occur due to the interaction of mean and recirculating flows. Long et al. [3] experimentally studied flow characteristics in the submerged jump based on the LDA measurements of velocity and turbulence components for various submergence factors and Froude numbers. They reported that the vortical structure near the gate to be the main source of the "climb effect" in velocity components. Dey and Sarkar [4] analysed ADV measurements of mean velocity components, Reynold stresses and turbulence intensity in submerged wall jet associated with the sudden change from smooth to rough bed. Experimental results indicate that the self-preserving feature of the flow appears in the fully developed region for smooth and rough bed conditions. In a latter study by Dey and Sarkar [5], experimental studies were conducted for similar flow characteristics as in the former study to investigate the mean velocity components, Reynold stresses and turbulence intensity components, as well as shear stress distributions along the rough bed. Their experimental studies revealed that the rate of jet decay in the submerged jump increases with an increase in bed roughness and thus the flow structure on rough and smooth beds were not identical. Gümüş et al. [6] conducted experimental and numerical studies to examine water surface profiles under submerged hydraulic jump conditions with different Froude numbers. Results indicated that the RNG turbulence model was in the highest agreement with the experimental results in comparison to other turbulence closure models.

In an open channel flume with smooth and horizontal bed in Figure 1(a), magnitude of the submerged wall jet can be assessed by the Froude number defined underneath the gate as $F_r = U_1/\sqrt{gy_1}$, where g is the gravitational acceleration, y_1 and U_1 are the water depth and average flow velocity under the gate, respectively. Corresponding subcritical conjugate depth can be calculated using Belanger equation $y_2 = 0.5y_1\left(\sqrt{1+8F_r^2}-1\right)$ based on the assumptions of inviscid flow and hydrostatic pressure distribution. The hydraulic jump forms beneath the free surface when the tail water depth y_t becomes greater than the conjugate depth y_2 and the corresponding submergence ratio can be evaluated with the submergence factor $S = (y_t - y_2)/y_2$ (e.g., [7]). Interaction of the incident flow with the recirculating flow in this region creates temporally and spatially varying vortices, which may result in significant

hydrodynamic effects such as lift forces at the gate lip and drag forces on the downstream face of the gate.

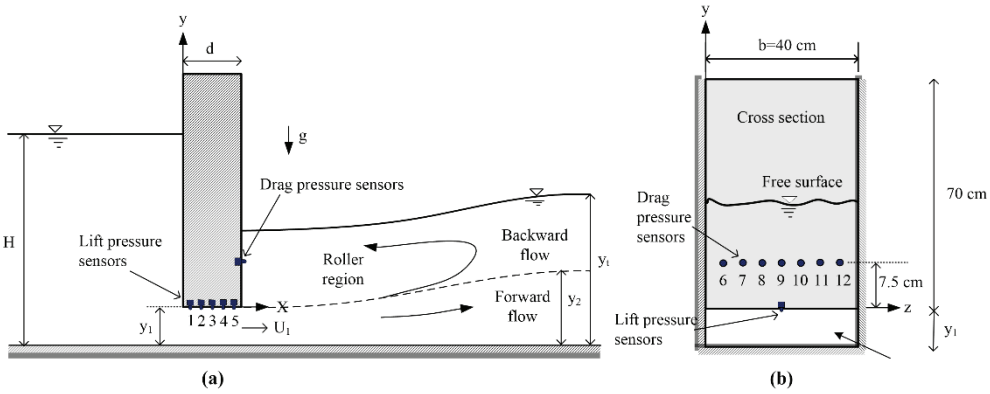

Figure 1 - Schematic representation of the submerged jump downstream of a vertical gate, (a) side view; and, (b) front view of the gate. Pressure sensors were embedded at the gate lip and downstream face of the gate

Several investigators have focused on the characteristics of hydrodynamic effects acting on different hydraulic structures. Thang and Naudascher [8] examined vortex-excited vibration of underflow vertical lift gates. They found that the dynamic interaction between elastic gate and unstable shear layer created a vortex that may force the gate to oscillate. Characteristics of the interaction process were analysed based on the spectral analysis of the hydrodynamic forces and the response of the gate. Bhargava and Narasimhan [9] carried out experimental studies to analyse hydrodynamic effects on the gate lip with various geometries. Time-averaged and fluctuating pressure coefficients were investigated using different Froude numbers and gate openings. They concluded that the gate lip with inclination less than 45º reduced the tendency of flow towards the separation. Geometry of the gate lip having 45º sloping lip with sharp and rounded upstream edges evidently provided the best reduction of total mean and fluctuating pressures. Fiorotto and Rinaldo [10] conducted experimental studies to investigate the pressure fluctuations under hydraulic jumps. They explored that the pressure at the jump location was maximum for *Fr=0.5*. Roth and Hager [11] carried out experimental studies to investigate the flow under the gates. Viscosity and surface tension effects, as well as pressure distributions on the channel bottom were discussed in detail. Corner vortices created by the stagnation flow near the gate were successfully suppressed by introducing a novel anti-vortex element mounted on the gate. Billeter and Staubli [12] experimentally studied flow-induced multiple-mode vibration of the submerged sluice gate. They used LDA and miniature pressure transducer to measure velocity and pressure simultaneously. Authors concluded that the self-excited vibration with the range of reduced velocity from 0.8 to 14 and the transition to galloping produced instability-induced excitation. The interaction between two different instability-induced vibrations was strongly dependent on the frequency ratio and the velocity range. Amir et al. [1] studied hydrodynamic effects on the sediment particle in free-surface flows using pressure sensors and PIV. Results showed that spatial and temporal scales in pressure fluctuations were relevant to the flow

depth and bed slope. Erdbrink et al. [13] conducted experimental studies to reduce the cross-flow vibration of underflow gates using resistance-type water level and force meter equipment. Experimental results on the submerged gate with low gate openings showed that the leakage flow approach could significantly reduce vibrations. Kampel et al. [14] experimentally studied the pressure fluctuations on the underflow gate due to the generation of upstream vortices. They concluded that the reduction of mean hydrodynamic pressure and increment in pressure fluctuations depended on the location of the longitudinal corner vortex upstream of the gate. Smok and Demirel [15] carried out experimental studies under different flow conditions of jet Froude number and submergence factor in order to provide how the vortex induced pressure fluctuations affect the gate stability. Results show that the fluctuation components are high at the leading and trailing edges of the gate due to the separation effects below the gate. Also Smok [16] investigated the hydrodynamic characteristic of lift and drag pressures on the submerged sluice gate, performing experimental studies under different flow conditions of Froude number, submergence factor and gate opening. Dios et al. [17] experimentally examined the behaviour of three-dimensional flow structure using ADV and PTV. Various Froude numbers and submergence factors were considered to analyse the mean velocity components and turbulence statistics. Velocity magnitude and turbulent kinetic energy were found to be significantly dependent on the submergence factor and Froude number. Bijankhan et al. [18] investigated velocity profiles downstream of the sluice gate using ADV and electromagnetic flowmeter for high submerged flow conditions. They concluded that the interaction of the energy correction factors and head loss values provided accurate results in head-discharge evaluation.

These studies reveal that the vortical structure around the submerged gate may result in hydrodynamic loads on the gate. The objective of the present study is to address how the gate responds to the vortical flow created by the submerged hydraulic jump under different flow conditions. Experimental studies were conducted in a laboratory flume for various Froude numbers, submergence factors and gate openings. Pressure fluctuations acting on the gate lip and downstream of the gate were measured simultaneously using pressure sensors at multiple locations. The contribution of the vortices to the wall pressures on the gate is examined by means of power spectrum analysis of instantaneous pressure measurements.

1.1. Experimental Setup and Pressure Measurement

Experimental studies were carried out in a rectangular flume of 10 m long, 65 cm high and 40 cm wide with transparent glass sidewalls and stainless-steel bottom. The head tank is used at the inlet of the flume to maintain a constant head at the upstream of the control structure. Water was supplied by a feeding pipe connected to the head tank. The flow discharge in the flume was controlled by using a valve located at the entrance of the head tank and monitored precisely using the ultrasonic flowmeter mounted on the feeding pipe. Tail water depth was controlled using a tilting gate located downstream of the flume.

The vertical rectangular gate was installed at the location 3.5 m away from the inlet section of the flume in order to avoid unsteady effects at the inlet. The sluice gate was designed with 70 cm of height, 12 cm of width and 38 cm of cross section with 1 cm of thickness of the steel bars at the sides. On the sidewalls, the opening between the channel and gate have been secured by silicone to prevent water leakage. Gate model was designed taking into account

laboratory conditions and device features such as gate thickness and minimum distance required for the connection of sensors. As seen in Fig. 2, five lift pressure sensors and seven drag pressure sensors were embedded at the centreline of the gate bottom and downstream side of the gate, respectively. These sensor arrays enabled to evaluate spatial variations of lift and drag pressures acting on the gate. Lift pressure sensors at the bottom of the gate were located at distances of 19, 41, 61, 81 and 101 mm from the upstream corner of the gate. Drag pressure sensors from 6 to 12 were located at horizontal distances of 6, 11, 15.5, 20, 24.5, 29 and 34 cm from the reference coordinate system shown in Figure 1(b). The geometry and dimensions of the gate were selected such that adverse hydrodynamic effects would be prominent. Thus the present experimental setup is not representative of an operating gate. Modelling studies conducted on large gates have been examined in detail in technical reports of USBR and a real scale gate design has been developed applying similarity models. The ratio of y_0 / B was determined as 1.308 from the dimensional analysis based on 16 physical parameters. Here, y_0 is the upstream water depth and B is the gate width [19]. This ratio was calculated as 1.71 for the present gate model, which is similar to the previously reported prototype case. Lip extension tests were carried out for 20, 40, 60 and 80% of gate width. It was reported that the lip length could be changed between 7.6 cm and 30.4 cm. Thus, width of the present gate remains in this range.

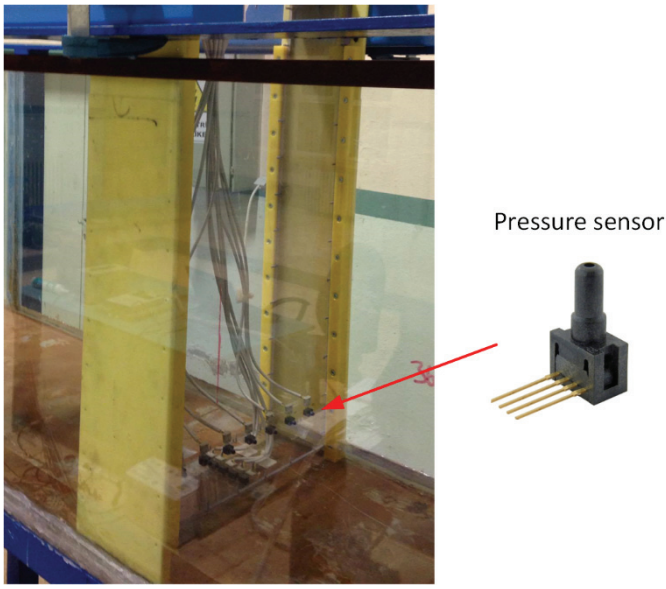

Figure 2 - Vertical gate equipped with multi-pressure sensors

Scale effects may be significant in the laboratory studies of engineering problems such as air-water flows in hydraulic jumps, void fraction, interfacial velocity, bubble count rate, turbulence intensity and bubble chord time [20]. In the present experimental setup, large eddies in the roller region may produce smaller hydrodynamic forces on the gate due to the scale effects.

The National Instrument data acquisition system (NI USB 6343 series) was used to measure the voltage signal from the stationary pressure sensors. The output voltage signal is collected by connecting the sensor pins to analogue input channels of data logger and to power supply. Measurements of pressure fluctuations were made by using the Honeywell pressure sensors (24PC-EFA6G series) as shown in Figure 2. These gage sensors, made from the fluorosilicone and straight type, have a full-scale range of 0 to 3450 Pa. The response of the pressure variation is typically supplied by 10 V directional current (DC) and the response time of 1 ms is justified by the manufacturer. Pressure sensors measure the pressure with respect to ambient pressure and hydrodynamic pressures cause the differential voltage to change. In order to facilitate stable pressure measurement, the cables connected to the pins of pressure sensors were configured into the side of the gate. The cables wired from sensor pins was then hooked up to the block hole of pre-barrier steel plate of the gate. The voltage signals in each pressure sensors were experimentally measured during 6 minutes in order to acquire adequate data for time averaging. A current regulator was integrated to the experimental setup in order to prevent noise effects originating from the electricity infrastructure network.

Static calibration test for the pressure sensor was conducted in a cubic water tank in order to justify the pressure gradient with the water depth and obtain an equation for the conversion of the voltage output to the pressure. A cubic water tank was designed and manufactured using 40 cm height and 30 cm × 30 cm surface bottom of plexiglass, Fig 3 (a). This test was performed in the range of 2 cm to 30 cm of water height in the calibration device by measuring the output voltage from pressure sensor in LabVIEW configuration. Every sensor has a different starting voltage depending on the manufacturing conditions. Thus, the voltage signals were proportionally and individually converted to the pressure using the best linear fit obtained from the measured data.

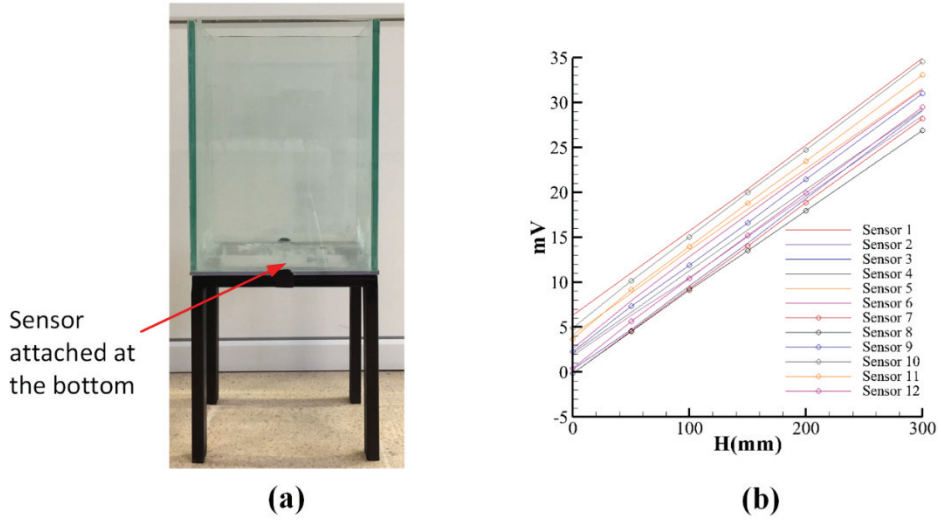

Figure 3 - (a) Static calibration test device; and, (b) variations of the voltage output with water depth for each sensor

Pressure sensor was dynamically calibrated on a draining cubic tank when the water depth in the tank is 30 cm initially. As depicted in Fig. 4, experimental measurements are compared with the available analytical results which were based on the inviscid flow assumption by Streeter et al. [21]. Analytical solution predicts a rapid draining at the early stage due to the neglected viscous effects. As the draining process develops with time, experimental measurements approach to the analytical results. The present dynamic calibration test shows that the present sensors are sensitive to the hydrodynamic conditions.

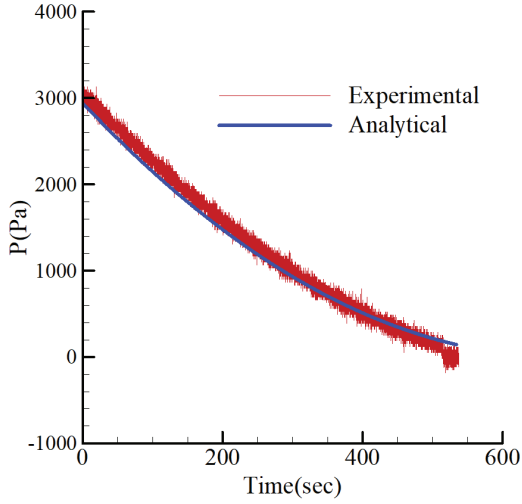

Figure 4 - Comparison of experimental measurements and analytical results during draining of the tank.

2. METHODOLOGY

2.1. Pressure Coefficients

Time-averaged and instantaneous wall pressures are evaluated using the following dimensionless pressure coefficients suggested by Bhargava and Narasimhan [9]:

$$C_{\bar{p}} = \frac{\left(H - \frac{\bar{p}}{\gamma}\right)}{\frac{U_1^2}{2g}} \tag{1}$$

$$C_{p'} = \frac{\sqrt{\overline{p'^2}}}{\frac{1}{2}\rho U_1^2}\frac{y_t}{H} \tag{2}$$

Where $C_{\bar{p}}$ is mean pressure coefficient, $C_{p'}$ instantaneous pressure coefficient, H is the upstream water depth, $\bar{p}$ is the time-averaged pressure, γ is the specific weight of water (= ρg), ρ is the density of water, U_1 is the average flow velocity under the gate and $\sqrt{\overline{p'^2}}$ is the

root mean square of pressure fluctuations. Bhargava and Narasimhan [9] found that the pressure fluctuations collapsed into a single curve for various values of y_t/H. Thus, the term y_t/H is included in Eq. (2).

2.2. Experimental Conditions

In order to investigate the hydrodynamic response of the gate to the vortex induced fluctuations, experimental studies were carried out under different flow conditions of gate opening, submergence factor and jet Froude number. The pertinent variables describing the flow conditions are calculated and summarized in three different groups in Table 1 to analyse the effects of key parameters describing the submerged hydraulic jump in a systematic manner. In the first group of experiments, various gate openings are considered for constant submergence factor and incident Froude number. To see the effect of submergence ratio, various submergence factors are adjusted for constant Froude number and gate opening in the second experimental set. In the last set, effect of jet Froude number was investigated for constant gate opening and submergence factor. These experimental conditions are tagged and depicted in the first column of Table 1, showing the first number as the group number and the second number as the run of the experiment in each set. Eleven experimental runs were carried out for the evaluation of mean and instantaneous wall pressures.

Table 1 - Flow parameters and dimensionless numbers for different experimental runs

Run	Q (m^3/s)	H(m)	y_1(m)	V_1(m/s)	Fr	y_2 (m)	y_t(m)	S
1.1	0.013	0.279	0.025	1.3	2.625	0.081	0.146	0.8
1.2	0.0171	0.336	0.03	1.425	2.627	0.097	0.175	0.8
1.3	0.0215	0.415	0.035	1.536	2.626	0.114	0.205	0.8
1.4	0.0263	0.495	0.04	1.644	2.624	0.13	0.234	0.8
2.1	0.015	0.33	0.025	1.5	3.029	0.095	0.152	0.6
2.2	0.015	0.35	0.025	1.5	3.029	0.095	0.172	0.8
2.3	0.015	0.38	0.025	1.5	3.029	0.095	0.19	1.0
3.1	0.013	0.279	0.025	1.3	2.625	0.081	0.146	0.8
3.2	0.015	0.35	0.025	1.5	3.029	0.095	0.172	0.8
3.3	0.017	0.441	0.025	1.7	3.433	0.110	0.197	0.8
3.4	0.019	0.516	0.025	1.9	3.837	0.123	0.223	0.8

Instantaneous pressure data obtained from the pressure sensors were filtered by using moving-average method. The moving-average method first takes the average of a subset with a specified windows size *w,* and then the fixed size of the subset is shifted forward successively to filter the entire raw data using the following equation (e.g., [22]):

$$Y(z) = \frac{b(1) + b(2)z^{-1} + ... + b(n_b + 1)z^{-n_b}}{1 + a(2)z^{-1} + ... + a(n_a + 1)z^{-n_a}} X(z) \quad (3)$$

The numerator and denominator coefficients in Eq. (3) are calculated as b = ones(1,w)/w and a = 1 in Matlab. The form of the dimensional digital moving average is functionally modified in Matlab programming [23] as y = filter(b, a, x), where x is the raw pressure data in vector form. In the present study, the window size was selected as w = 100 with respect to the pressure noise condition and a feedback from the autocorrelation procedure. The window size is determined by trying different values and selecting the value at which the data is removed from the noise at the most appropriate level. Time variations of raw and filtered pressures are represented in Fig. 5 (a) and Fig. 5 (b) for sensors 3 and 9, respectively, located in the middle of the gate lip and downstream face.

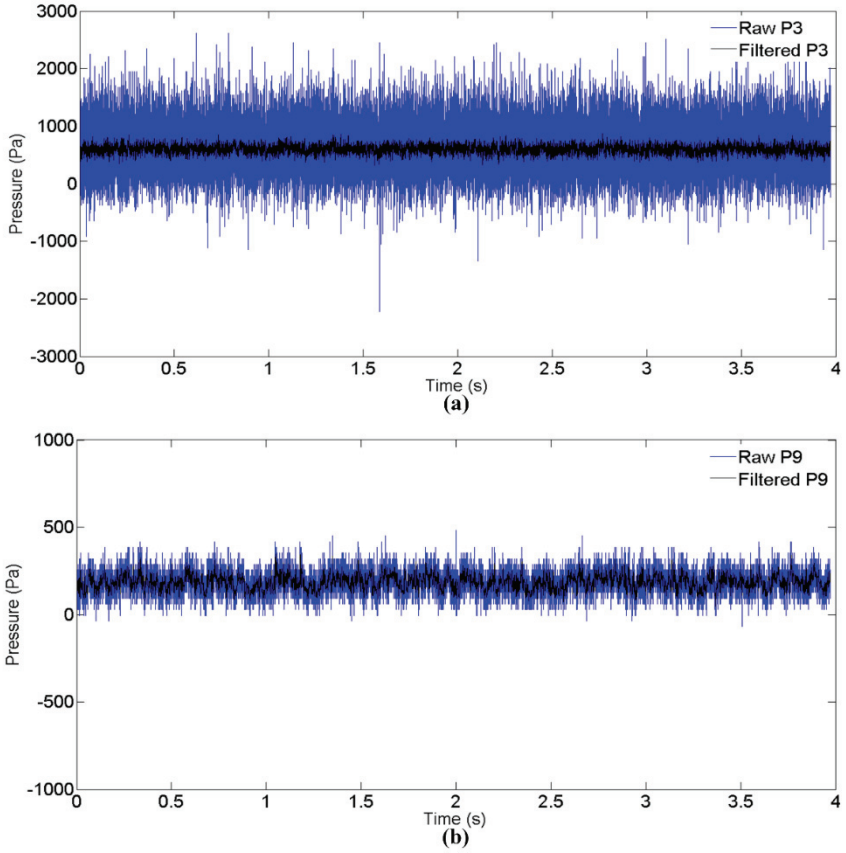

Figure 5 - (a) Comparison of raw and filtered pressure data for: (a) lift; and, (b) drag pressures (Fr = 3.029)

3. RESULTS AND DISCUSSIONS

3.1. Lift Pressures

Instantaneous pressures were measured simultaneously at five different locations on the gate bottom for different flow conditions given in Table 1. It should be noted again that the frequency of each pressure sensor was 1000 Hz during experimental measurements. Gate opening is a critical parameter for the hydrodynamic response of the submerged gate even for constant Froude numbers since the same Froude number can be provided with different gate openings. Fig. 6 depicts the mean pressure variations at the gate lip. It can be observed that the minimum and maximum pressure magnitude ranges increase at relatively greater gate openings and pressures at the trailing edge of the gate decrease constantly due to the decreasing gate opening. The stagnation point is determined at $x/d=0.667$ for $y_1=0.03$ and $y_1=0.025$ (Fig. 1). The positions of the different variables will be defined with the expression x/d. The effect of the gate opening is observed to be more pronounced at the trailing edge of the gate at low gate openings. This observation suggests that the interaction of incoming jet with the recirculating flow has significantly reduces the pressure at the trailing edge of the gate, even for the same Froude number and submergence factor.

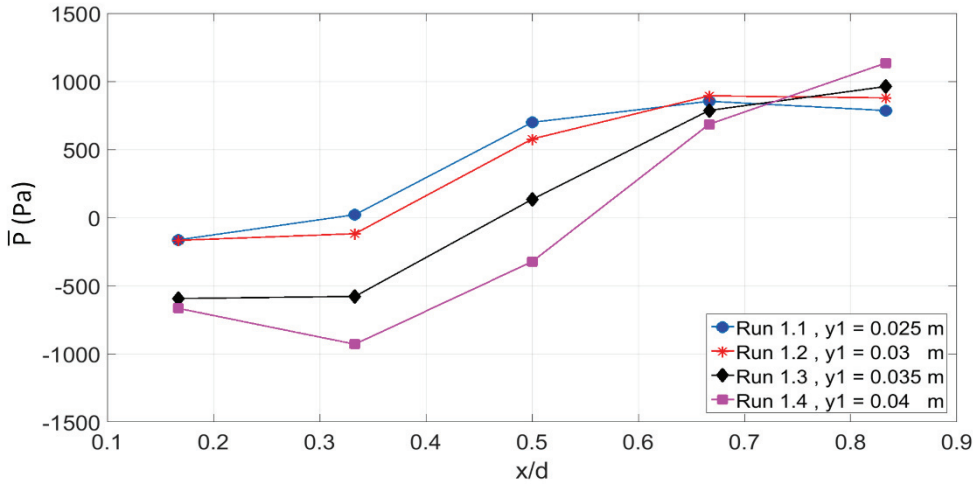

Figure 6 - Comparison of mean pressure variations at different locations on the gate lip for various gate openings (Fr = 2.63 and S = 0.8)

Spatial variations of time-averaged and instantaneous pressure coefficients at the gate lip are shown in Fig. 7 for different gate openings. Spatial coordinates of the measurement points are non-dimensionalised with the thickness of the gate. The minimum $C_{\bar{p}}$ occurs at x/d=0.667 for, y_1=0.025 whereas the location of the minimum $C_{\bar{p}}$ shifts to the downstream edge of the gate as the gate opening increases. Notice that the minimum $C_{\bar{p}}$ corresponds to the maximum pressure coefficient. The location of the maximum $C_{p'}$ in Fig. 7(b) apparently depends on the gate opening. The maximum value of $C_{p'}$ occurs just downstream of the leading corner of

the gate for y_1=0.04. The starting points of $C_{p'}$ values were almost at the same locations for all gate openings. On the contrary, the interaction of the backward flow with the incident flow significantly increased the pressure fluctuations at higher gate openings.

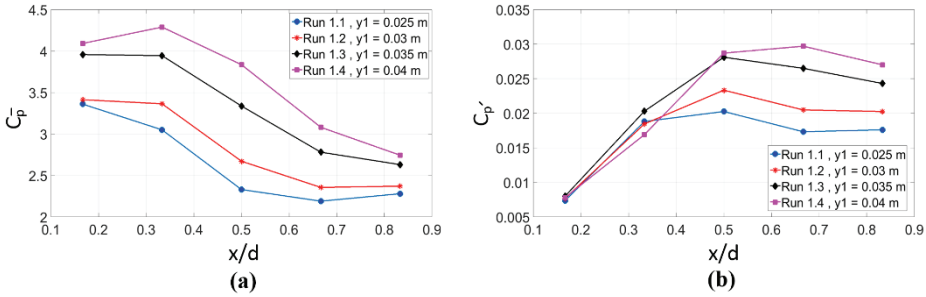

Figure 7 - Spatial variations of (a) mean; and, (b) fluctuating pressure coefficients along the gate bottom for various gate openings (Fr = 2.63 and S = 0.8)

Fig. 8 shows the mean pressures at different locations on the gate lip for various submergence factors. Froude number and gate opening were kept constant to investigate the effect of downstream conditions on the lift pressures. It can be concluded from the figure that the hydrodynamic pressures are almost proportional to the submergence ratio. Comparison of the pressure magnitudes at each measurement point shows that the separated flow from the upstream leading edge reattaches to the gate bottom to increase the pressure at the downstream edge of the gate. Magnitudes of hydrodynamic pressures at the leading edge are less than that at other measurement points since the accelerating flow at the entrance of the gate opening causes the pressure magnitudes to reduce in this region.

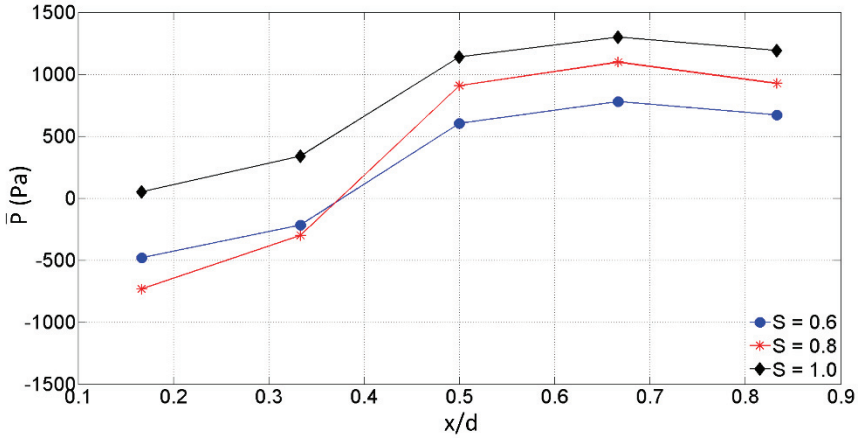

Figure 8 - Comparison of mean pressure variations at different locations on the gate lip for various submergence factors (Fr = 3.029 and y_1 = 0.025 m)

Spatial variations of time-averaged and fluctuating pressure coefficients along the gate bottom are shown in Fig. 9 for various submergence factors. The uncertainty in experimental data is customarily represented using error bars. In 10% of cases used the error bar on the 90% confidence interval. Time-averaged pressure coefficients synchronized at similar values with the submergence factor and takes the minimum value at the point *x/d=0.667* of the gate bottom. Error bar values of S = 0.6 and 0.8 show similar trends along the gate bottom in terms of mean pressure coefficient. When the comparison is made according to the maximum value of the submergence factor 1; it has been observed that varying submergence factors have the greatest effect on the mean pressure coefficient at the upstream and downstream corners of the gate. Scattering of the mean pressure near the leading and trailing edges of the gate lip associated with the separation pocket below the gate, which was also observed by Bhargava and Narasimhan [9] experimentally. The spatial distributions of the $C_{p'}$ along the gate bottom in Fig. 9(b) show that the pressure fluctuations increase as the submergence factor decreases. The peak value of the $C_{p'}$ is observed at the middle of the gate. The strong interaction of the recirculating flow with the incoming flow at low submergence caused higher pressure fluctuations. As the submergence factor increases, the effect of the downstream flow conditions disappears. It can be observed from Fig. 9(b) that pressure fluctuations depend on the submergence factor between upstream corner and middle of the gate. The uncertainty in $C_{p'}$ values were similarly represented using error bars with 90% confidence interval. Here, pressure coefficients along the gate bottom are independent of the submergence ratio and differences converge to a constant value.

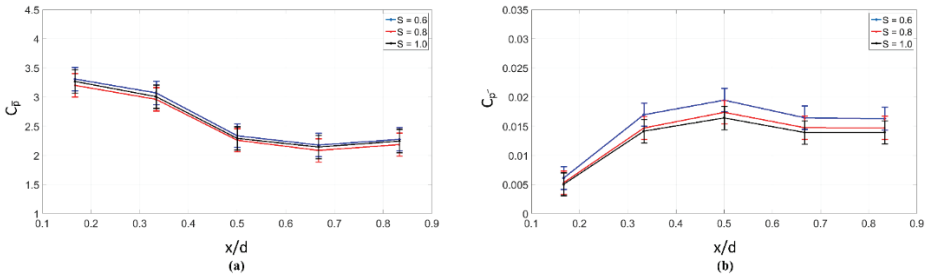

Figure 9 - Spatial variations of (a) mean; and, (b) fluctuating pressure coefficients along the gate bottom for various submergence factors (Fr = 3.029 and y_1 = 0.025 m)

Spatial variations of time-averaged pressure coefficient along the centerline of the gate lip are given in Fig. 10(a) for different Froude numbers. In Eq. (1), the low mean pressure coefficient corresponds to a high mean pressure. It can be seen in Fig. 10(a) that the time-averaged pressure coefficient decreases as the Froude number increases due to the increasing upstream water depth. Moreover, the 90% confidence interval of mean pressure coefficients with Froude number is effective only in the middle of the gate. The uncertainty analysis on the fluctuating pressure coefficient shows that the effect of the Froude number increases along the gate. While the $C_{p'}$ values are in the same range, the difference grows near the downstream corner of the gate and varies depending on the Froude number.

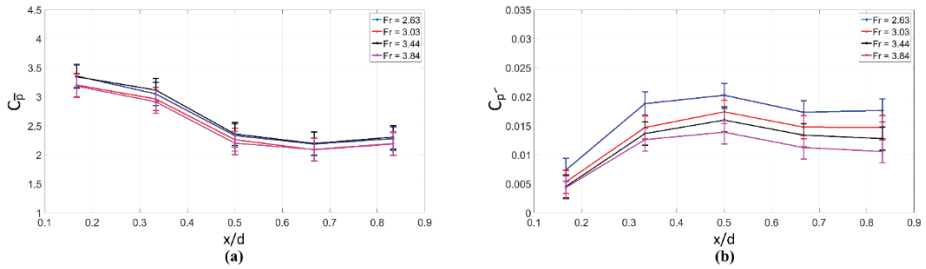

Figure 10 - Spatial variations of (a) mean; and, (b) fluctuating pressure coefficients along the gate bottom for various Froude numbers (S = 0.8 and y_1 = 0.025 m)

The minimum mean pressure coefficient is observed immediately downstream of the center of the gate lip (*x/d*=0.667) due to the impingement of the separated flow from the upstream corner. Therefore, the location of a minimum mean pressure coefficient corresponds to a stagnation point at the gate bottom. High $C_{\bar{p}}$ values downstream of the stagnation point are associated with the accelerating flow in this region. The confidence interval boundary (CIB) values for spatial variations of mean; and, fluctuating pressure coefficients along the gate bottom for various submergence factors are given in Table 2.

Table 2 - The confidence interval boundary values for spatial variations of mean; and, fluctuating pressure coefficients along the gate bottom for various submergence factors

Run		x/d=0.167		x/d=0.333		x/d=0.5		x/d=0.667		x/d=0.833	
		Up CIB	Low CIB	Up CIB	Low CIB	Up CIB	Low CIB	Up CIB	Low CIB	Up CIB	Low CIB
2.1	$C_{\bar{p}}$	3.478	3.144	3.226	2.918	2.453	2.219	2.285	2.067	2.388	2.16
	$C_{p'}$	0.0064	0.0058	0.0178	0.0161	0.0204	0.0185	0.0173	0.0156	0.0171	0.0155
2.2	$C_{\bar{p}}$	3.361	3.041	3.109	2.813	2.372	2.146	2.189	1.98	2.293	2.074
	$C_{p'}$	0.0055	0.005	0.0154	0.0139	0.0182	0.0165	0.0155	0.014	0.0154	0.0139
2.3	$C_{\bar{p}}$	3.432	3.105	3.158	2.857	2.406	2.177	2.249	2.035	2.357	2.132
	$C_{p'}$	0.0053	0.0047	0.0148	0.0134	0.0172	0.0156	0.0146	0.0132	0.0146	0.0132
3.1	$C_{\bar{p}}$	3.525	3.189	3.2	2.895	2.446	2.213	2.294	2.075	2.39	2.163
	$C_{p'}$	0.0077	0.0069	0.0197	0.0178	0.0212	0.0192	0.0182	0.0165	0.0185	0.0167
3.2	$C_{\bar{p}}$	3.361	3.041	3.109	2.813	2.372	2.146	2.189	1.98	2.293	2.075
	$C_{p'}$	0.0055	0.005	0.0154	0.0139	0.0182	0.0165	0.0155	0.014	0.0154	0.0139
3.3	$C_{\bar{p}}$	3.511	3.176	3.271	2.96	2.475	2.24	2.302	2.083	2.418	2.188
	$C_{p'}$	0.0047	0.0045	0.0143	0.0136	0.0167	0.0159	0.014	0.0133	0.0134	0.0127
3.4	$C_{\bar{p}}$	3.342	3.024	3.057	2.766	2.309	2.089	2.195	1.986	2.303	2.083
	$C_{p'}$	0.0045	0.0043	0.0132	0.0126	0.0146	0.0138	0.0118	0.0112	0.011	0.0105

3.2. Drag Pressure

Instantaneous pressures were measured at different locations on the downstream face of the gate (Fig. 1(b)) during the experimental studies. Spatial variations of the time-averaged and instantaneous pressure coefficients on the downstream face of the gate are shown in Fig. 11

for various Froude numbers. The time-averaged pressure coefficient is slightly higher at the near edges. This suggests that the time variation of the vorticity field downstream of the gate does not result in a symmetrical mean pressure field on the gate. The minimum time-averaged pressure coefficient occurs at the center of the gate. The vortex pair observed downstream of the gate creates a low momentum region at the center of the gate. The same behaviour is observed in the spatial variation of the instantaneous pressure coefficient $C_{p'}$ on the gate. Unsteady motion of the vortex pair downstream of the gate created an almost symmetrical behaviour in both mean and instantaneous pressure coefficients. The maximum $C_{p'}$ values occur at $z/b \approx 0.28$ and $z/b \approx 0.72$ at which location the recirculation effects were found to be significant from the span-wise measurements of velocity profiles downstream of the submerged gate by Long et al. [3]. This suggests that the surface pressure fluctuations on the gate are closely connected with the vortical flow in the roller region downstream of the gate.

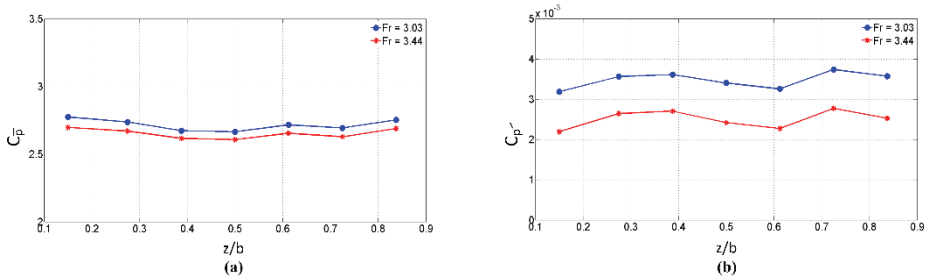

Figure 11 - Spatial variations of (a) mean; and, (b) fluctuating pressure coefficients along the downstream face of the gate for various Froude numbers

Spatial variations of the mean and instantaneous pressure coefficients on the downstream face in Fig. 12 reveal the same non-symmetrical distribution along the span-wise direction for different gate openings. The maximum $C_{p'}$ occurs at $z/b \approx 0.38$ again and the magnitude of the $C_{p'}$ increases as the gate opening increases. This again suggests that the fluctuating pressure coefficient strongly depends on the gate opening, as displayed in Fig. 11(b). Vortex induced pressure fluctuations on the downstream face of the gate increased with the gate opening. The position of the peak of the $C_{p'}$ is independent of the flow condition.

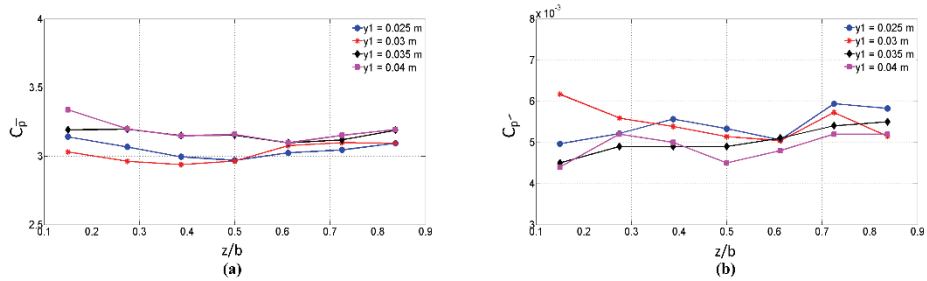

Figure 12 - Spatial variations of (a) mean; and, (b) fluctuating pressure coefficients along the downstream face of the gate for various gate openings

$C_{\bar{p}}$ values pursue a constant magnitude range throughout the gate for different gate openings and same Froude number. According to the complex recirculation flow region, $C_{p'}$ magnitudes have also fluctuating behaviour along the downstream of the gate. Considering the low extent, $C_{p'}$ values were not highly differ from each other for different gate openings. Fig. 12 indicates that the changing velocities due to the constant Froude number and different gate openings have a direct relation with the pressure magnitudes.

3.3. Frequency Spectra

The power spectrum obtained from the instantaneous pressure measurements were employed in order to examine the contribution of the vortices to the wall pressure fluctuations on the gate. The power spectrum analysis was performed using Welch [24] method. The frequency spectra of lift pressure fluctuations are shown in Fig. 13 for Fr = 3.837 with constant submergence factor and gate opening. The spectral magnitude at P1 which is the closest pressure sensor to the leading edge experiences a peak frequency at 14.65 Hz and then starts to decrease until the high-frequency range of 170 Hz. For the other lift sensors, significant peaks were not observed at a low-frequency range and the magnitude only increases at 200 Hz then decays synchronized with a distinct slope. The low-pressure magnitudes at the leading and trailing edges of the gate lip produce less spectral level due to the accelerating flow in this region. The reliability of the collected data was provided after repeated experiments.

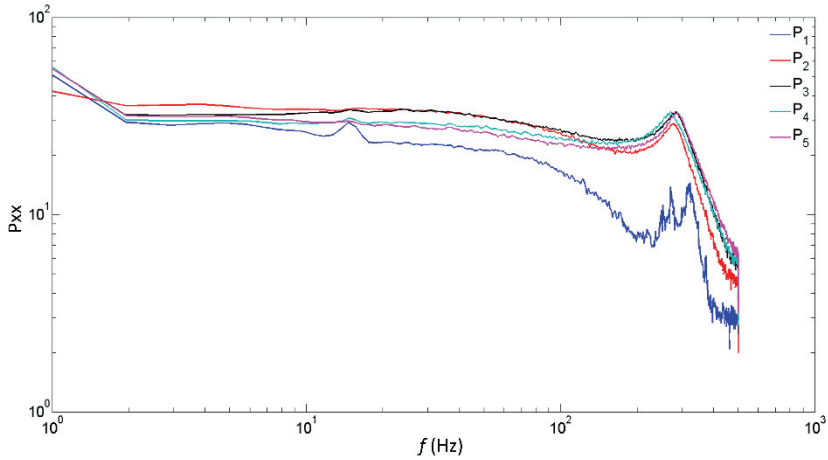

Figure 13 - Spectra of lift pressure fluctuations for Fr = 3.837, S = 0.8 and y_1 = 0.025 m

The estimated frequency spectra for lift and drag pressure fluctuations were spatially averaged on the lip and downstream face of the gate, respectively. Fig. 14 shows the averaged power spectrum of lift pressure fluctuations for various Froude numbers in order to see the effect of Froude number on the spectral behaviour. The dominant frequency is observed within the range of 14-19 Hz for all cases, and for the Froude numbers of 2.625 and 3.029

dominant frequencies are also observed at around 40, 55 and 95 Hz. The largest spectral contributions to lift pressures occur at approximately between the frequency of $f \cong 14, f \cong 19$ Hz for various Froude numbers. As the Froude number increases, the dominant frequency shifts to the higher frequencies and the spectral magnitude diminishes with a constant slope in the high-frequency region. This suggests that contributions of the recirculation effects to the lift pressures decreases as the Froude number increases for a constant gate opening and submergence factor since the flow jet with high momentum can suppress recirculation effects. Thus, the low Froude number flow experiences high pressure fluctuations in the low-frequency region. As shown in Fig. 14, the spectral decay follows the Kolmogorov power law as $f^{-5/3}$ in the high-frequency range.

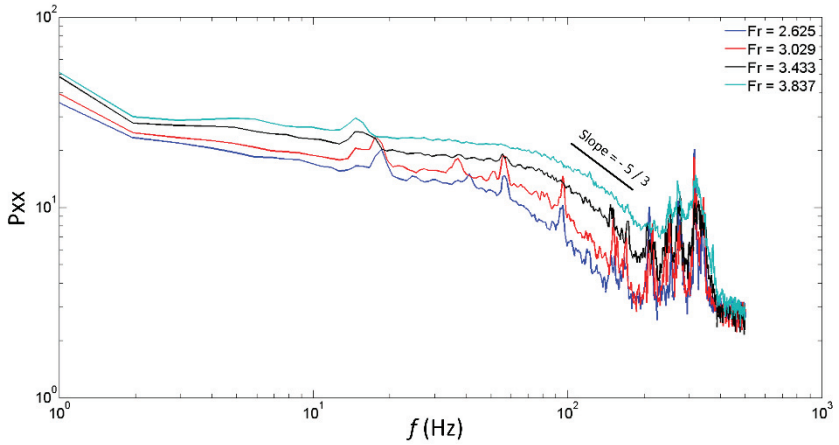

Figure 14 - Spatially averaged spectra of lift pressure fluctuations for various Froude numbers (S = 0.8 and y_1 = 0.025 m)

Spatially averaged lift and drag pressure fluctuations are compared for different Froude numbers in Fig. 15. The spectra of drag pressure fluctuations roll off more sharply compared to the lift pressures in the low-frequency range. The energy level of the lift pressure fluctuations is larger than that of the drag pressure fluctuations. Lift and drag pressure fluctuations contain the peak energy at the same frequency close to 13 Hz for Fr = 3.837. The power spectra of drag pressure fluctuations in the high-frequency range show unstable behaviour which may be attributed to the high frequency surface wave fluctuations in the vicinity of the gate.

The power spectra of lift pressure fluctuations are compared in Fig. 16 for free and submerged flow conditions. It can be clearly seen in the figure that the interaction of the recirculation flow with the mean flow induces lift pressure fluctuations on the gate lip. However, a significant spectral level is not observed for the free flow conditions. This observation suggests that when the gate is subjected to the submerged hydraulic jump, recirculating flow downstream of the gate may give rise to increase hydrodynamic effects below the gate. It should be noted here that drag pressure fluctuations are not available for free flow conditions.

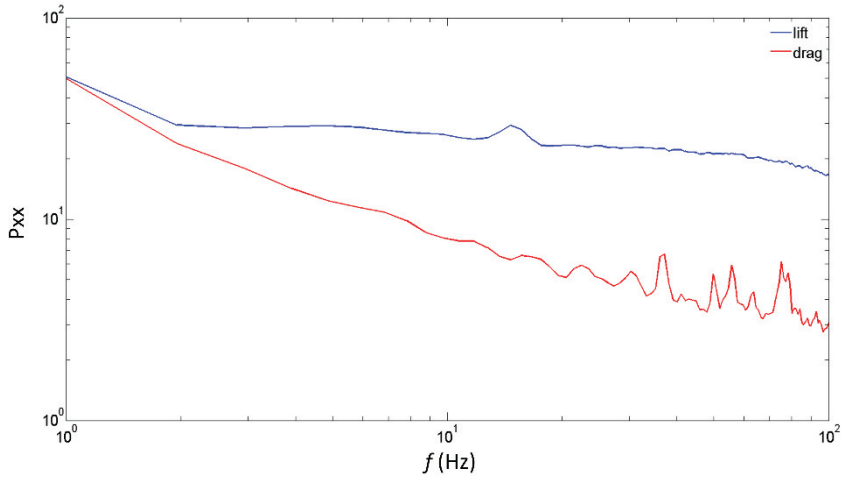

Figure 15 - Comparison of spatially averaged power spectra of pressure fluctuations for Fr = 3.837, S = 0.8 and y_1 = 0.025 m

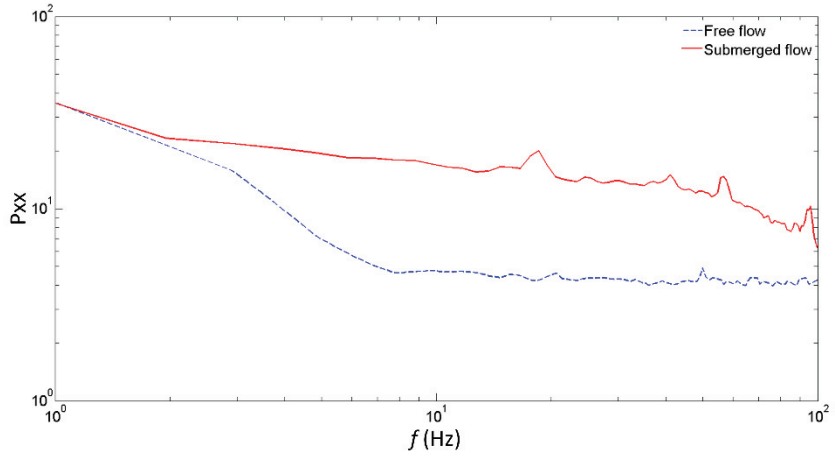

Figure 16 - Comparison of spatially averaged power spectra of lift pressure fluctuations for submerged and free flow conditions (Fr = 2.625 and y1 = 0.025 m.)

4. CONCLUSIONS

Laboratory studies were carried out by means of instantaneous pressure measurements to investigate surface pressure fluctuations on the gate under various flow conditions. Experimental results enabled to gain insights on the contributions of vortices to the pressure fluctuations acting on the control structure. The experimental system used in this study can be classified as a large gate model in terms of model scale.

For low Froude number flows, backward flow downstream of the gate interacts with the separated flow and significantly affects the pressure fluctuations near the upstream corner of the gate bottom. The minimum mean pressure coefficient along the gate lip is observed immediately downstream of the center of the gate lip due to the impingement of the separated flow from the upstream corner. Interaction of the flow jet with the recirculating flow significantly reduces the pressure magnitude near the downstream corner of the gate, even for the same Froude number and submergence factor. On the other hand, the position of the maximum of the instantaneous pressure coefficient occurs at the center of the gate lip independently from the gate opening. The position of the minimum pressure coefficient close to the downstream of the gate attributed to a stagnation point. Stagnation points were observed significantly at relatively narrow gate openings such as 3 cm and 2.5 cm. The vortex pair observed downstream of the gate creates a low momentum region at the center of the gate. Unsteady motion of the vortex pair downstream of the gate shows non-symmetrical distributions of mean and instantaneous drag pressure coefficients. The maximum instantaneous pressure coefficients were observed at the same location where recirculation effects were found significant from the previous span-wise velocity measurements downstream of the submerged gate in the literature. This suggests that the surface pressure fluctuations on the gate are closely connected with the vortical flow in the roller region downstream of the gate.

Experimental results of this study show that the power spectra of drag and lift pressure fluctuations are found to decay with different slopes in the low-frequency range. Results show that different Froude number flows experience the same frequency fluctuations as in the low-frequency region and additional frequency fluctuations occur in the high-frequency region for the low Froude number. The power spectra of lift pressure fluctuations are devoid of any significant spectral level over a wide frequency range for the free flow conditions. Findings from this experimental study suggest that the hydrodynamic features of the control structures in irrigation systems need to be monitored using pressure sensors depending on the seasonal operational and downstream conditions. The experimental analysis described in this study can be used by engineers to increase economic life of hydraulic structures based on the monitoring of hydraulic infrastructures. Hydrodynamic pressure measurements reported in this study can also be used to validate high resolution numerical models, which may be used for the simulation of turbulent flows through real scale submerged gate flows.

Symbols

$C_{\bar{p}}$: Mean pressure coefficient

$C_{p'}$: Instantaneous pressure coefficient

d : Gate width

Fr : Froude number

g : Gravitational acceleration

H : Upstream water depth

$\overline{p'^2}$: Pressure fluctuation

$\bar{p}$: Time-averaged pressure

S : Submergence factor

U_1 : Average flow velocity

w : Window size

y_1 : Upstream water depth

y_2 : Downstream water depth

y_t : Tail water depth

γ : Specific weight of water

Acknowledgements

This work was supported by the Scientific and Technological Research Council of Turkey (TUBITAK) under Grant no. 216M521.

References

[1] Amir, M., Nikora, V.I., Stewart, M.T., Pressure forces on sediment particle in turbulent open-channel flow: A laboratory study. J. Fluid Mech., 757, 458-497, 2014.

[2] Svendsen, I.A., Veeramony J., Bakunin J., Kirby, J.T., The flow in weak turbulent hydraulic jumps. J. Fluid Mech., 418, 25-57, 2000.

[3] Long, D., Steffler, P.M., Rajaratnam N., LDA study of flow structure in submerged hydraulic jump. J. Hydraul. Res., 28, 437-460, 1990.

[4] Dey, S., Sarkar, A., Response of velocity and turbulence in submerged wall jets to abrupt changes from smooth to rough beds and its application to scour downstream of an apron. J. Fluid Mech., 556, 387-419, 2006.

[5] Dey, S., Sarkar, A., Characteristics of turbulent flow in submerged jumps on rough beds. J. Eng. Mech., 134, 49-59, 2008.

[6] Gümüş, V., Aköz, M.S., Kırkgöz, M.S., Kapak mansabında batmış hidrolik sıçramanın deneysel ve sayısal modellenmesi. Teknik Dergi, 24(117), 2013.

[7] Rajaratnam, N., Advan J. Hydraulic jumps. Hydro-Sci, 4, 197-280, 1967.

[8] Thang, N.D., Naudascher, E., Vortex-excited vibration of underflow gates. J. Hydraul. Res. 24, 133-151, 1986.

[9] Bhargava, V.P., Narasimhan, S., Pressure fluctuation on gates. J. Hydraul. Res., 27, 215-231, 1989.

[10] Fiorotto, V., Rinaldo, A., Turbulent pressure fluctuations under hydraulic jumps. J. Hydraul. Res., 30, 499-520, 1992.

[11] Roth, A., Hager, W.H., Underflow of standard sluice gate. J. Exp. Fluid., 27, 339-350, 1999.

[12] Billeter, P., Staubli, T., Flow-induced multiple-mode vibrations of gates with submerged discharge. J. Fluids. Struct., 14, 323-338, 2000.

[13] Erdbrink, C.D., Krzhizhanovskaya, V.V., Sloot, P.M.A., Reducing cross-flow vibration of underflow gates: Experiments and numerical studies. J. Fluid. Struct., 50, 25-48, 2014.

[14] Kampel, I., Prenner, R., Krouzecky, N. Pressure fluctuations on underflow gates of weirs due to upstream vortex generation. Materials Today: Proceedings., 4, 5833-5838, 2017.

[15] Smok, S., Demirel, E., Pressure Measurements on the Gate Subjected to Submerged Hydraulic Jump. Advances in Fluid Mechanics, Ljubljana, Slovenia, 2018.

[16] Smok, S. Experimental Investigation of Vortex Induced Hydrodynamic Effects Acting on the Submerged Gate and Development of Vortex Breaker Apparatus, Master Thesis, Eskişehir Osmangazi University, 2019.

[17] Dios, M., Bombardelli, F.A., Garcia, C.M., Liscia, S.O., Lopardo, R.A., Parravicini, J.A., Experimental characterization of three-dimensional flow vortical structures in submerged hydraulic jumps. J. Hydro-Environ. Res., 15, 1-12, 2017.

[18] Bijankhan, M., Kouchazadeh, S., Belaud, G., Application of the submerged experimental velocity profiles for the sluice gate's stage-discharge relationship. Flow. Meas. Instrum., 54, 97-108, 2017.

[19] Murray, R.I., Simmons, W.P., Hydraulic Downpull Forces on Large Gates. Bureau of Reclamation, Report Number Research Report No. 4., 1966.

[20] Murzyn, F., Chanson, H., Experimental assessment of scale effects affecting two-phase flow properties in hydraulic jumps. Exp. Fluids, 45, 513-521, 2008.

[21] Streeter, V. L., Wylie, E. B., Bedford, K. W., Fluid Mechanics, 9ed, McGraw-Hill, US, 1998.

[22] Oppenheim, A.V., Schafer, R.W., Buck, J.R., Discrete-time signal processing, Upper Saddle River, New Jersey, 1999.

[23] The MathWorks, Pro-Matlab User's Guide. South Natick, MA, 1990.

[24] Welch, P.D., The use of fast Fourier transforms for estimation of power spectra: A method based on time averaging over short, modified periodograms. IEEE Transactions on Audio and Electroacoustic, 15, 70-73, 1967.